An Identification Problem in Electromyography

June 21, 2021

Abstract

In medical treatment, it can be necessary to know the position of a motor unit in a muscle. Recent advances in high-density surface Electromyography (EMG) measurement have opened the possibility of extracting information about single motor units. We present a mathematical approach to identify these motor units. On the base of an electrostatic forward model, we introduce an adjoint approach to efficiently simulate a surface EMG measurement and an optimal control approach to identify these motor units. We show basic results on existence of solutions and first-order optimality conditions.

Keywords: nonlinear optimization in function spaces, electromyography, biomedical modeling, identification problem in medical application

1 Introduction

In the human body, muscles are responsible for movement. These muscles consist of many muscle fibers, which are organized in so-called motor units. A motor unit is thereby the smallest controllable unit of the muscle. When we use a muscle, one or more of these motor units are activated by the peripheral nervous system. This activation causes electrical signals, so-called action potentials, to propagate along the muscle fibers. These propagating action potentials create a spatially and temporally changing potential field. One can measure this potential by electrodes, placed on the skin above the muscle.

A fundamental question in medical research and diagnosis is: what is the bioelectric source that is responsible for a specific measured potential on the skin? To answer this question, one has to find a way to identify these sources from the given measurements. Such an identification of bioelectric activity from surface measurement is needed in many fields of medicine, e.g., in measuring brain activity (EEG) or cardiac activity (ECG). Correspondingly, a lot of work has been performed to develop tools for computational assistance, see, e.g., [16] and references therein for EEG. In general terms, refinements of classical Tychonov regularization techniques are applied to the spatial problem.

The corresponding technique for the identification of action potentials in muscles is called electromyography (EMG). It can be used for purpose of research (which motor-unit is responsible to which movement?) or in pre-operative planning (where is the location of important nerves, which should not be harmed in operations?). Similar techniques as described above have also been applied to electromyography measurements [20, 31, 32]. These techniques yield a smooth, distributed reconstruction of sources, which is appropriate in those applications where the sources are smoothly distributed within the tissue. In these approaches, mainly spatial problems are solved, not taking into account the spatio-temporal structure of the problem.

However, bioelectrical sources in motor units are known to have special structure. They consist of a characteristic action potential that is concentrated along a line in space and moves along a fiber. Approaches that directly attempt to process the spatio-temporal information and exploit the high temporal resolution of surface EMG are less common. A notable exception is [23]. The authors consider a regularized least-squares approach for fitting the EMG signal by a linear combination of a moderate number of analytically predefined and prelocated waveforms.

The aim of our work is to establish a mathematically sound approach to the EMG problem that, similarly to [23], takes into account the special structure of moving action potentials in muscles. Similar to [23], we use a least-squares tracking type functional for the identification. However, we introduce refined approaches to simulate a surface EMG measurement from a given source. We also represent the source to be identified more flexible via a curve that can be chosen freely inside the muscle tissue.

Using a quasi-static approach, cf. [26], one can simulate for fixed time t the potential Φ, which is generated from the moving action potential, by solving a Poisson equation of the form

$$\int_{\overline{\Omega}} (\sigma(x)\nabla\Phi(x,t)) \cdot \nabla v(x)\,\mathrm{d}x + \int_{\partial\Omega_S} \mu\Phi(s,t)v(s)\,\mathrm{d}s = \int_{\overline{\Omega}} v(x)\,\mathrm{d}\rho(t). \tag{1}$$

In this setting, the time dependent source density $\rho(t)$, which is given through a moving action potential, is spatially concentrated on the motor unit and thus modeled as a measure, concentrated on a line. Solutions to this problem in the sense of Stampacchia can be found in $W^{1,p'}(\Omega)$ where $p > d$ and $1/p + 1/p' = 1$, cf. e.g., [28] and a discussion concerning uniqueness can be found in [24]. However, the direct numerical solution of (1) for all t in the time interval of interest would incur high computational cost, i.e., for each time instant an elliptic PDE on a three-dimensional domain would have to be solved. That would render numerical approaches to the identification problem too costly. We overcome this difficulty by an adjoint approach and reduce the simulation of a single measurement via (1) to the evaluation of a line integral.

Based on this simulation model, we establish a least-squares type tracking problem to identify the motor units from a surface EMG measurement. Subject of our identification problem is the trajectory of the moving action potential, represented by a parameterized curve. Unlike the least-squares approach in [23], our problem is formulated in an infinite-dimensional function space setting, which makes the analysis of the problem much more involved. Those kinds of infinite-dimensional optimization problems emerge in many application-related problems. Therefore, the prototype of this problem is studied very well, cf. e.g., [18,30,35] and we will employ techniques of analysis established in the field of research to show existence of solutions and first order optimality conditions. This lays the groundwork for an optimization based numerical approach to our identification problem. A detailed elaboration of such an approach, however, will not be subject to the current paper.

2 Modeling of a Surface Electromyography Measurement

Our first aim is to simulate a surface EMG measurement . Thus, for a given electric charge $\rho(t)$ we would like to simulate the measurement of an electric potential $y(t) \in \mathbb{R}$, by an electrode, located on the skin.

For this simulation, we first have to derive mathematical models for the quantities of interest. First, we describe how those parts of the human body, where the motor unit lies, can be modeled mathematically. Then there is a physical model that describes the connection between the

potential we want to simulate and the source that is responsible for it. We also need a model for the action potential, which acts as the source term.

As we will see, there are two problems when we simulate an surface EMG measurement. First, we will notice that the computation is costly and not efficient. To overcome this problem, we introduce an adjoint approach. Secondly, there appear so-called end-effects, modeling artifacts, which can disturb the identification. Therefore, we present a way to reduce these effects.

2.1 A Mathematical Model of Human Tissue

We start with a mathematical description of the human body. To avoid computational overhead, we consider only a locally truncated part, containing the region of interest. This is a reasonable assumption, since static electric fields decay quickly far away from the source.

To represent some part of the body geometrically, we choose a bounded open domain $\Omega \subset \mathbb{R}^3$ with Lipschitz boundary $\partial\Omega$. That means locally, $\partial\Omega$ is the graph of a Lipschitz continuous function. One can find a more detailed definition, e.g., in [8,30]. Since the human body consists of different tissue types, we split the domain Ω into several subdomains Ω_i, such that $\Omega = \cup\Omega_i$. For simplicity's sake, we restrict our model to three different tissue types, namely muscle, fat, and bone tissue. We use Ω_M, Ω_F, and Ω_B as notation. Thereby, the index M stands for muscle tissue, the index F for fat tissue, and the index B for bone tissue. From the truncation, we get an artificial boundary, which we call $\partial\Omega_A$. Last but not least, skin tissue bounds the rest of our domain, and we label it with $\partial\Omega_S$. We suppose that the skin part has positive measure, such that we can place electrodes on the skin. Thus it yields

$$\partial\Omega = \partial\Omega_S \cup \partial\Omega_A, \qquad \emptyset = \partial\Omega_S \cap \partial\Omega_A.$$

In the human body, each tissue type has three different electromagnetic properties. Those properties are the conductivity σ, the permittivity ϵ, and the permeability μ. First, we note human tissue is not magnetic. Thus the permeability is given by the permeability of vacuum μ_0. We also know that the upper frequency limit in human tissue is around $1kHz$, see [21, 22, 26]. In this frequency range, one can assume that the tissue is purely resistive. Thus the properties are independent of the exact frequency, see [21, 29]. Furthermore, it is known that bone and fat tissue are isotropic, concerning conductivity and the permittivity. In contrast, muscle tissue is anisotropic. There the conductivity and permittivity are higher in the direction of the muscle fibers, see [1, 21, 29]. Both properties depend, therefore, on the geometry of the muscle. For simple geometries, one can assume that the muscle fibers are straight or at least only slightly curved. Therefore, we can define, for example, the x-axis as the axial direction and rotate the geometry such that the motor unit is approximately parallel to the x-axis. Thus we can represent them by a 3×3 matrix. To be consistent, we write the conductivity and permittivity as a scaled identity matrix if the tissue is isotropic. In Tabular 1, we listed the conductivity and permittivity values for different tissue types. Note that the permittivity is given relatively to the permittivity of vacuum, which is $\epsilon_0 = 8.8\text{e}{-12}\ \frac{A\ s}{V\ m}$. Since the conductivity is constant within each tissue type we can make the following two estimates, needed for ellipticity and boundedness of the bilinear form in (1):

$$\sigma^{\max} := \max\{\|\sigma^M\|_\infty, |\sigma^F|, |\sigma^B|\} < \infty \tag{2}$$

$$\sigma^{\min} := \min\{\lambda_{\min}(\sigma^M), |\sigma^F|, |\sigma^B|\} > 0. \tag{3}$$

tissue type	fat	bone	muscle (axial)	muscle (radial)	skin
conductivity [S/m]	4.0e−2	2.0e−2	4.0e−1	9.0e−2	1.0
permittivity [rel.]	1.5e5	-	2.0e7	4.4e6	5.5e4

Table 1: Conductivity and permittivity for different tissue types, see [33].

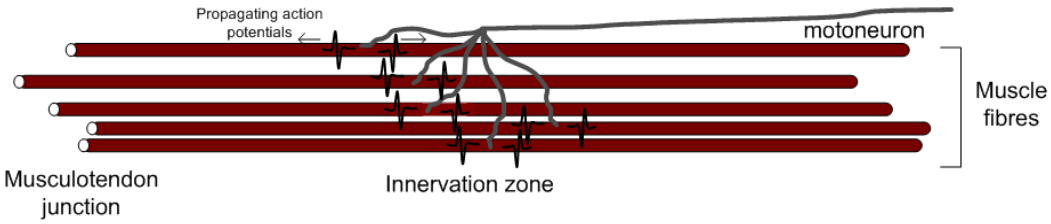

Figure 1: Sketch of a motor unit

Last but not least, we have to derive a mathematical description of the motor unit. In bioelectricity, a motor unit is a bundle of muscle fibers. In Figure 1 one can see a sketch of a motor unit. Motor units are the smallest entities within a muscle that can be controlled individually by the brain. First, our brain sends a signal to the neuromuscular junction, which lies in the innervation zone of the muscle. The innervation zone lies thereby in the middle of the muscle. When a motor unit is activated, it generates two action potentials that propagate towards both ends of the motor unit, see [14] and cause a contraction of the muscle cells along the way. These propagating action potentials also create an electric potential in the whole tissue, which can be measured on the skin. One can assume that the activation of the muscle fibers in a motor unit happens simultaneously, see [21]. Thus the superposition principle holds, and we can treat a motor unit as a single fiber. We represent such a single fibered motor unit by a regular curve $u \in H^2(-1,1,\mathbb{R}^3)$. We denote by $u(0)$ the neuromuscular junction and by $u(-1)$ and $u(1)$ the two ends of the motor unit.

2.2 A Quasi-Static Model of the Electric Potential

A surface EMG measurement device measures the electric potential at the skin that is caused by a moving electric charge within the motor unit. To simulate a measurement we need a model that connects a moving electric charge with the corresponding electric potential in the tissue. The velocity of these moving charges is relatively slow, such that electrodynamic effects (like emission of electromagnetic waves) can be neglected. Thus, we will use a quasi-static model, see [21, 26].

We denote the moving electric charge by $\rho(x,t)$, and the corresponding potential by $\Phi(x,t)$, where x is the spatial variable and t the time. Then, in classical form we obtain the following model, which would have to be augmented by boundary conditions and transmission conditions to take into account jumps of σ at material boundaries:

$$-\operatorname{div}\sigma(x)\nabla\Phi(x,t) = \rho(x,t), \tag{4}$$

see [26]. Moreover, we will model the action potential as a moving charge along a fiber, which is a curve in 3D. So $\rho(\cdot,t)$ is rather a measure than a function in x. We will thus proceed to derive an appropriate weak form of (4).

As mentioned above, there are two different boundary types, namely $\partial\Omega_S$, which represents the

skin, and $\partial\Omega_A$, which is an artificial boundary, caused by the truncation of the domain. For $\partial\Omega_S$ we assume that there are no other sources outside of the domain, and thus the potential is zero there. Those assumptions lead to the following Robin boundary condition

$$\sigma(x)\nabla\Phi(s,t)\cdot\nu+\mu\Phi(s,t)=0 \quad \text{ at } \partial\Omega_S,$$

where $\mu>0$ is the skin conductivity. For $\partial\Omega_A$, we also assume that no other sources are present in the rest of the body. That means we can use homogeneous Neumann boundary conditions in this case:

$$\sigma(x)\nabla\Phi(s,t)\cdot\nu=0 \quad \text{ at } \partial\Omega_A.$$

Combining these aspects, formal integration by parts yields the following symmetric bilinear form

$$\begin{aligned} a &: H^1(\Omega)\times H^1(\Omega)\to\mathbb{R} \\ a(\Phi,v) &:= \int_\Omega (\sigma(x)\nabla\Phi(x))\cdot\nabla v(x)\,\mathrm{d}x+\int_{\partial\Omega_S}\mu\Phi(s)v(s)\,\mathrm{d}s. \end{aligned} \tag{5}$$

Due to the presence of Robin boundary conditions with $\mu>0$ on $\partial\Omega_S$, this bilinear form is $H^1(\Omega)$-elliptic by a generalized Poincare inequality, cf. e.g., [30, Lemma 2.5]. Thus, by the Lax-Milgram theorem, we obtain a continuously invertible linear operator

$$\begin{aligned} A &: H^1(\Omega)\to H^1(\Omega)^* \\ (A\Phi)(v) &:= a(\Phi,v). \end{aligned}$$

Since $H^1(\Omega)$ is reflexive, we may identify $H^1(\Omega)^{**}\cong H^1(\Omega)$ and also consider the adjoint operator $A^*:H^1(\Omega)\to H^1(\Omega)^*$ of A as $(A^*v)(\Phi)=a(\Phi,v)=(A\Phi)(v)$.

As already mentioned, we will model the electric charge at a time-instant t by a measure $\rho(t)\in\mathcal{M}(\overline{\Omega})\sim C(\overline{\Omega})^*$ on $\overline{\Omega}$. Thus, we may introduce the following weak form:

$$a(\Phi(t),v)=\int_{\overline{\Omega}} v d\rho(t) \quad \forall v\in C^\infty(\overline{\Omega}). \tag{6}$$

Since $H^1(\Omega)\not\hookrightarrow C(\overline{\Omega})$ in our 3D-setting, we cannot write (6) as an operator equation $A\Phi(t)=\rho(t)$ in $H^1(\Omega)$, and thus the Lax-Milgram theorem cannot be applied directly. Nevertheless, by an approach due to Stampacchia, see [28], solvability of (6) with $\Phi(t)\in W^{1,p'}(\Omega)$ for some $p'<3/2$ can be established.

In this approach the bilinear form (5) is redefined on different spaces as

$$a_p : W^{1,p'}(\Omega)\times W^{1,p}(\Omega)\to\mathbb{R}$$

with $1/p+1/p'=1$ for $p>3$, implying that $W^{1,p}(\Omega)\hookrightarrow C(\overline{\Omega})$. This gives rise to the following restricted pre-dual problem for some $l\in W^{1,p'}(\Omega)^*\hookrightarrow H^1(\Omega)^*$:

$$\text{find } \psi\in W^{1,p}(\Omega) : a_p(v,\psi)=l(v) \quad \forall v\in H^1(\Omega).$$

By Lax-Milgram, this problem has a solution $\psi\in H^1(\Omega)$, and it is a question of regularity theory, if ψ is an element of $W^{1,p}(\Omega)$. If this is true for all $l\in W^{1,p'}(\Omega)^*$, which is known as "maximal regularity", then the pre-dual operator

$$\begin{aligned} {}^*A_p &: W^{1,p}(\Omega)\to W^{1,p'}(\Omega)^* \\ ({}^*A_p\psi)(v) &= a_p(v,\psi) \end{aligned}$$

is an isomorphism by the open mapping theorem.

Remark 1. *More generally, it can be shown that ψ is an element of $H^1(\Omega) \cap C(\overline{\Omega})$ if $l \in W^{1,p'}(\Omega)^*$, cf. e.g. [17]. Then, with some additional technical effort, we can still show solvability of* (6)*, but an additional criterion is required to single out a unique solution. A detailed discussion can be found in [24].*

For simplicity we thus impose the following assumption:

Assumption 2.1. *The domain Ω and its subdomains Ω_j are sufficiently regular, such that the operator ${}^*A_p : W^{1,p}(\Omega) \to W^{1,p'}(\Omega)^*$ is an isomorphism for some $p > 3$.*

Under this assumption and by reflexivity of Sobolev spaces, we can conclude that the adjoint of $A_p := ({}^*A_p)^*$

$$\begin{aligned} A_p : W^{1,p'}(\Omega) &\to W^{1,p}(\Omega)^* \\ (A_p\phi)(w) &:= a_p(\phi, w) \end{aligned}$$

is also an isomorphism, since adjoints of isomorphisms in normed spaces are isomorphisms, as well.

Due to the continuous and dense embedding $W^{1,p}(\Omega) \hookrightarrow C(\overline{\Omega})$ we can use the corresponding adjoint embedding $C(\overline{\Omega})^* \hookrightarrow W^{1,p}(\Omega)^*$ to regard the charge $\rho(t)$ as an element of $W^{1,p}(\Omega)^*$ for each t, and we obtain unique solvability of the operator equation:

$$A_p\Phi(t) = \rho(t)$$

Hence, a unique electric potential $\Phi(t) \in W^{1,p'}(\Omega)$ that satisfies (6) exists for each $\rho(t)$. Since all spaces are reflexive, we can identify the adjoint operator and the pre-adjoint operator $A_p^* = {}^*A_p$.

2.3 Simulated Measurements by an Adjoint Approach

With the above model, the potential $\Phi(t)$ can in principle be computed in the whole domain for every t if $\rho(t)$ is given. However, the computational effort to do so with finite elements is too large, given that we are only interested in a certain number of measurements $y_i(t)$ at the boundary of Ω. We thus develop a more efficient adjoint approach to compute a desired measurement $y(t) \in \mathbb{R}$ from given $\rho(t)$.

In our setting, the potential is measured with small circular electrodes on the skin as follows

$$y(t) := B(\Phi(t)) = \frac{1}{|D|} \int_D \Phi(s,t)\, \mathrm{d}s,$$

where $D \subset \partial\Omega_S$ is the area of the electrode. The trace theorem, cf. e.g. [30, Theorem 2.1], implies that B is well defined as an element of $W^{1,p'}(\Omega)^*$.

Let $\rho(t) \in W^{1,p}(\Omega)^*$ and denote by $\Phi(t) \in W^{1,p'}(\Omega)$ the solution of

$$(A_p\Phi(t))(v) = \rho(t)(v) \quad \forall v \in W^{1,p}(\Omega). \tag{7}$$

Now consider the solution $\omega \in W^{1,p}(\Omega)$ of the adjoint problem:

$$(A_p^*\omega)(\phi) = B(\phi) \quad \forall \phi \in W^{1,p'}(\Omega). \tag{8}$$

Then we compute easily

$$y(t) = B(\Phi(t)) = (A_p^*\omega)(\Phi(t)) = a_p(\Phi(t), \omega) = (A_p\Phi(t))(\omega) = \rho(t)(\omega). \tag{9}$$

That means we can compute the potential at an electrode efficiently by evaluating

$$y(t) = \int_\Omega \omega(x)\, \mathrm{d}\rho(t). \tag{10}$$

where $\omega \in W^{1,p}(\Omega) \hookrightarrow C(\overline{\Omega})$ is the previously computed solution of the adjoint problem (8). In the following section, we will give a physiologically meaningful definition of the measure $\rho(t)$, concentrated on a curve, such that (10) can be evaluated as a line integral. Then the computation of $y(t)$ requires just the evaluation of this line integral, which is much cheaper than computing the solution of an elliptic equation. For several electrodes B_i, $i \in 1 \dots n_E$, we obtain $y_i(t)$ via solutions ω_i of the corresponding problems $A_p^* \omega_i = B_i$.

For our EMG problem, we may assume that the moving charge is completely contained in the muscular subdomain Ω_M, which is disjoint with the domains of measurement $D_i \subset \partial\Omega_s$. We can thus invoke regularity results to obtain more smoothness of the restriction $\omega|_{\Omega_M}$. This is useful to render sensitivities of $y(t)$ with respect to perturbations of the support of $\rho(t)$ well defined, which in turn are needed for our optimal control problem.

Lemma 2.2. *The solution ω of (8) is in $C^\infty(\Omega_M) \cap W^{1,p}(\Omega)$.*

Proof. Restricted to Ω_M, $\omega|_{\Omega_M}$ satisfies a Laplace equation, with $\sigma|_{\Omega_M}$ being constant and no sources are involved. Boundary conditions are given by $\omega|_{\partial\Omega_M}$. Such problems, however, are known to be C^∞ regular in the interior, cf. e.g. [12, Cor. 8.11]. □

2.4 Moving Action Potentials

In this section we provide a model for the charge $\rho(t)$ that moves along a fiber inside the motor unit. As described in section 2, the source density ρ is given by two action potentials moving along a motor unit. For simplicity, we assume that the measured data corresponds only to one active motor unit. This is a reasonable assumption, since it is possible to identify the activity of single motor units through EMG decomposition methods, see for example [19].

Since the radius of the fiber is very small, we will model our fiber as (the trace of) a fixed curve u in Ω_M. The action potential extends spatially along that fiber, but also moves along the fiber during the time span of the activation. The action potential takes a characteristic shape, sketched in Figure 2, and we have to map this signal onto a certain time varying segment of the curve that describes the fiber to obtain the line measure $\rho(t)$ at time t. Additional difficulties arise towards the ends of the fiber. Here special care has to be taken.

Biomedical modeling of action potentials starts with the following function

$$i_m(z) := \begin{cases} -c(\sigma_{in}, r) \exp(az) \left(6az + 6(az)^2 + (az)^3\right) & \text{if } z \le 0 \\ 0 & \text{else,} \end{cases} \tag{11}$$

in terms of a reference parameter $z \in \mathbb{R}$. Here $a > 0$ is a scaling factor that determines the spatial extension of the signal and $c(\sigma_{in}, r)$ is a constant depending on the intracellular conductivity σ_{in} and the radius of the motor unit r. For a more detailed description of the action potential we refer to [1, 21, 27]. One can easily verify that

$$I_m(z) := \begin{cases} -c(\sigma_{in}, r) \exp(az) \left(3(az)^2 + (az)^3\right) \frac{1}{a} & \text{if } z \le 0 \\ 0 & \text{else} \end{cases} \tag{12}$$

is the antiderivative of i_m an thus it can be observed that

$$\int_{\mathbb{R}} i_m(z)\ \mathrm{d}z = I_m(0) - \lim_{z\to-\infty} I_m(z) = 0,$$

which corresponds to the principle of conservation of charge in the body. Up to now, the action potential is defined as a function on $\mathbb{R}$, so the next step is to define a pull-pack of i_m onto the given curve $u \in \Omega_M$. A common assumption in biomedical modeling is that the velocity ν with which the action potential propagates along the fiber is constant, see [21]. Since the curve u represents the trajectory of the two propagating action potentials, we therefore choose the parameterization of the curve u such that it matches with the propagation velocity ν of the signal, in other words $|\dot{u}(\tau)| \equiv \nu$. That means we can identify each point on the curve u with some $z \in \mathbb{R}$ via the arc length

$$z(\tau) = \int_0^\tau |\dot{u}(\xi)|\,\mathrm{d}\xi = \int_0^\tau \nu\,\mathrm{d}\xi = \nu\tau.$$

That means $z(0) = 0$ corresponds to the neuromuscular junction $u(0)$ and we can identify points that are on the "right" side of the neuromuscular junction with some $z \in \mathbb{R}^+$ and points on the "left" side with some $z \in \mathbb{R}^-$. To model the action potential that propagates from the neuromuscular junction towards the "right" end of the fiber, we shift the origin of the action potential $i_m(z)$ by $\nu \cdot (t_0 - t)$ and set

$$\tilde{\rho}(u(\tau), t) = \begin{cases} i_m\left(z(\tau) + \nu \cdot (t_0 - t)\right)\right) & \text{if } z(\tau) > 0 \\ 0 & \text{else.} \end{cases}$$

To model the second action potential that propagates in the opposite direction, we mirror the signal at point zero, which is equal to adding a minus sign before $z(\tau)$ and changing $z(\tau) > 0$ to $z(\tau) < 0$. By combining both action potentials we get a line-measure ρ_l as follows:

$$\rho_l(u(\tau), t) := \hat{\rho}_l(\tau, t) := \left.\begin{cases} i_m\left(z(\tau) + \nu \cdot (t_0 - t)\right)\right) & \text{if } z(\tau) < 0, \\ i_m\left(-z(\tau) + \nu \cdot (t_0 - t)\right)\right) & \text{if } z(\tau) > 0 \end{cases}\right\} = i_m\left(\nu \cdot (|\tau| + t_0 - t)\right), \tag{13}$$

and since it $\hat{\rho}(\cdot, t)$ is continuous in τ we can write (10) as

$$\begin{aligned} y(t) &= \int_\Omega \omega(x)\,\mathrm{d}\rho_l(t) := \int_u \omega(x)\rho_l(x,t)\,\mathrm{d}s = \int_{-1}^1 \omega(u(\tau))\rho_l(u(\tau),t)\,|\dot{u}(\tau)|d\tau \\ &= \int_{-1}^1 \omega(u(\tau))\,\hat{\rho}_l(\tau,t)\nu\,\mathrm{d}\tau = \int_{-1}^1 \omega(u(\tau))\,i_m\left(\nu\cdot(|\tau| + t_0 - t)\right)\nu\,\mathrm{d}\tau. \end{aligned} \tag{14}$$

In Figure 2 we visualized the action potential and the support projected onto the curve for different time steps.

Conservation of charge and end-effects. As we have observed, our model i_m of the action potential respects conservation of charge in the sense that its total integral over $\mathbb{R}$ vanishes.

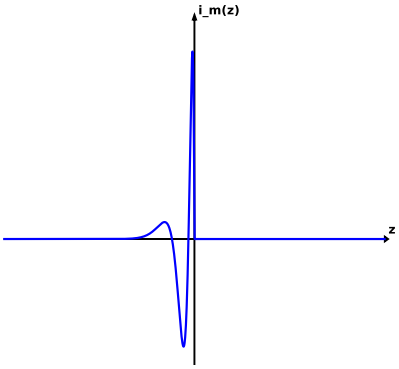

(a) Prototype of the action potential (12)

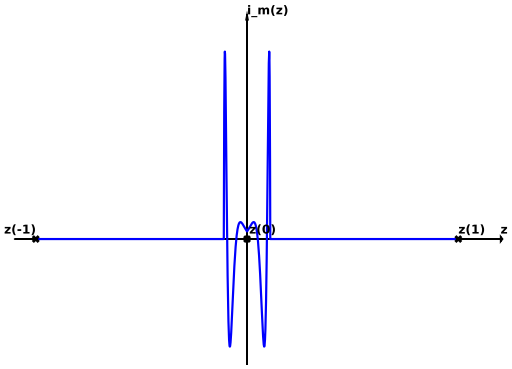

(b) Action potential truncated at the tail

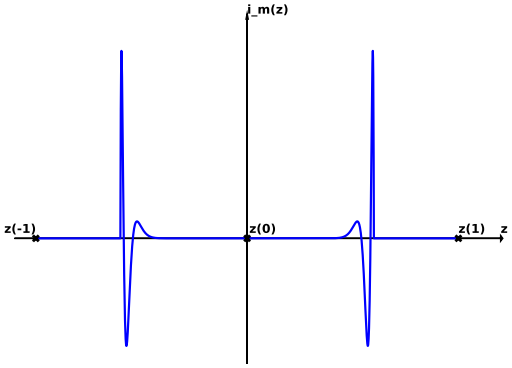

(c) Action potential with neglectable truncation

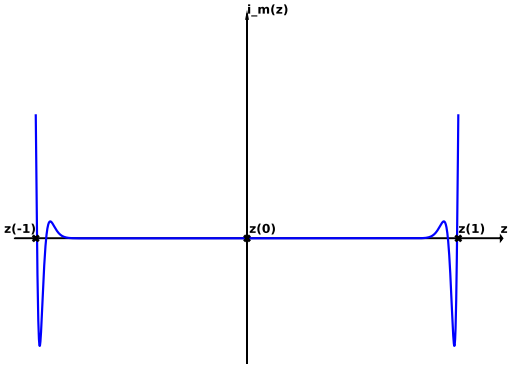

(d) Action potential truncated at the head

Figure 2: Action potential for different time instances

However, our definition of $y(t)$ involves only an integral over a bounded subset of $\mathbb{R}$ and the corresponding total charge is given by (taking into account the substitution of variables formula):

$$\begin{aligned}\rho_{total}(t) &= \int_{-1}^{0} i_m\left(\nu\cdot(-\tau+t_0-t)\right)\nu\,\mathrm{d}\tau + \int_{0}^{1} i_m\left(\nu\cdot(\tau+t_0-t)\right)\nu\,\mathrm{d}\tau \\ &= -I_m(\nu\cdot(-\tau+t_0-t))\Big|_{-1}^{0} + I_m(\nu\cdot(\tau+t_0-t))\Big|_{0}^{1}\end{aligned} \tag{15}$$

which is non-zero in general. This truncation of the integral, which can be observed in Figure 2 needs to be compensated for. Otherwise, the principle of conservation of charge would be violated and yield characteristic artifacts in simulations, so called *end-effects*. Those end effects can be observed in the red simulation of Figure 4c.

The representation of (15) by boundary terms at $\tau = -1, 0, 1$ already suggests how to construct an appropriate compensation. We will add point (Dirac) measures at $u(0)$, $u(1)$ and $u(-1)$, scaled by the negatives of the corresponding boundary terms to the measure $\rho(t)$. This can also be interpreted physiologically: at the ends of the fibers, transitional imbalances of charge are

compensated by small displacements of charge in the close vicinity of the end-plates. A similar approach can be found in [14].

When looking at the action in Figure 2b, one can observe that the first truncation of the action potential is at the neuromuscular junction. In (15) this corresponds to the boundary term at $\tau = 0$. Therefore we get

$$\rho_s(u(0), t) := 2I_m(\nu \cdot (t_0 - t)),$$

which is a Dirac measure at the neuromuscular junction $u(0)$. In Figure 2c one can observe that after some time the main part of the action potential lies on the motor unit, which means that the imbalance of charges coming from the truncation at the neuromuscular junction tends to zero, exponentially.

When the action potentials arrive at the ends $u(-1)$ and $u(1)$ of the motor unit, see action potentials in Figure 2d, they are again truncated. Thus we have to compensate the boundary terms at $\tau = -1$ and $\tau = 1$ in (15) by Dirac measures at $u(-1)$ and $u(1)$ as follows:

$$\rho_s(u(-1), t) = \rho_s(u(1), t) := -I_m(\nu \cdot (1 + t_0 - t)).$$

Observe that these charges are 0, if $t \leq 1 + t_0$, since $I_m(z) = 0$ for $z \geq 0$. In Figure 4c one can see a comparison of simulations of $y(t)$ with and without the source term compensation. Without compensation the simulated signal has two characteristic extra spikes (shown in red). These effects can be very pronounced, compared to the remaining signal, due to the smoothing effect of the potential equation. Our above described compensation technique can eliminate these end-effects, as seen in Figure 4c by observing the green function. By adding these stationary source terms, the compensated model (16) reads as follows:

$$\begin{aligned} y(t) &= \int_\Omega \omega(x) d(\rho_l + \rho_s)(t) \\ &= \int_{-1}^{1} \omega(u(\tau))\nu\rho_l(u(\tau), t)\, \mathrm{d}\tau + \sum_{\tau \in \{-1,0,1\}} \omega(u(\tau))\rho_s(u(\tau), t) \\ &= \int_{-1}^{1} \omega(u(\tau))\nu\hat{\rho}_l(\tau, t)\, \mathrm{d}\tau + 2\omega(u(0))\nu I_m(\nu(t_0 - t)) - (\omega(u(-1)) + \omega(u(1)))\, I_m(\nu(t_1 - t)). \end{aligned} \tag{16}$$

2.5 Numerical Simulation of a Surface EMG Measurement

To illustrate the properties of the forward problem, we perform the simulation of a surface EMG measurement, using the previously established model. We consider a measurement for a single fibered motor unit in the first dorsal interosseous (FDI) muscle of the right hand. At this point, we would like to thank the authors of [25] for sharing the STL files of their MRI measurements.

For simplicity, our model contains only the FDI muscle and the first two metacarpal bones. The rest of the domain was modeled as fat tissue. In Figure 3, the geometrical model is depicted. As one can see in Figure 3, there is a grid of 24 circular electrodes placed above the FDI muscle. We sketched the motor unit as a 2D projection onto the electrode grid by a black line. To incorporate the electrode grid into the STL files, we used the CAD software Blender [4]. To generate a mesh from the STL data, we used gmsh [11]. We performed all the following computations in C++,

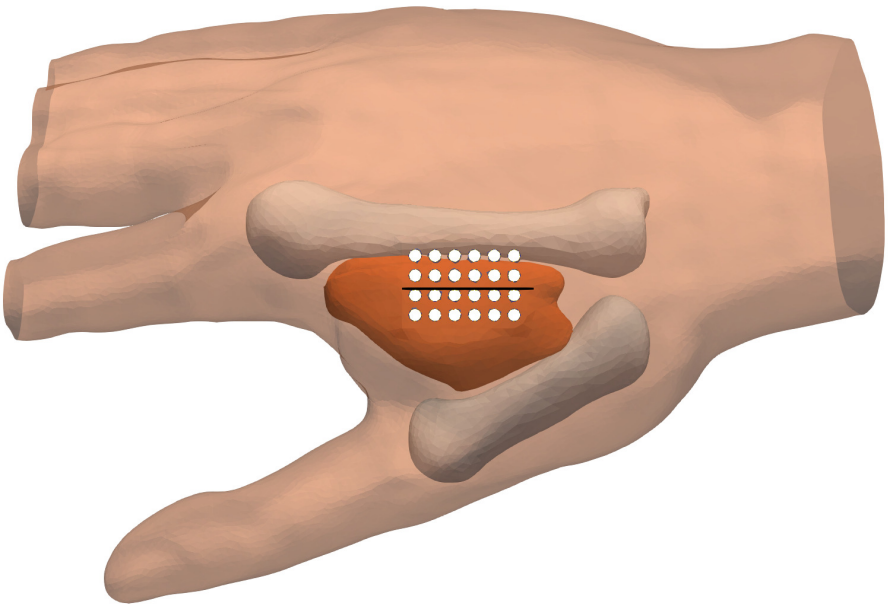

Figure 3: Geometrical setup for a numerical simulation: white dots: electrodes, dark brown: FDI muscle, light brown: bones and remaining tissue, black line: motor unit.

where we used the toolbox Dune [3] for all mesh-related operations, and the finite element toolbox Kaskade7 [15] to solve the adjoint problem.

The numerical computation of the adjoint solutions is done by a finite element method on a triangulation $\mathcal{T}$ of Ω consisting of 414195 tetrahedrons. On $\mathcal{T}$ we used continuous piecewise quadratic ansatz functions to discretize $W^{1,p}(\Omega)$ and $W^{1,p'}(\Omega)$ by

$$W_h := \{w \in C(\Omega, \mathbb{R}) : w|_K \in P_2(K)\ \forall K \in \mathcal{T}\}.$$

As usual we use then a Galerkin-Method to solve the adjoint problem (8), which lead to the discrete problem

$$\begin{aligned} &\text{find } \omega_h \in W_h \text{ s.t.} \\ &\quad (A_p^* \omega_h)(\phi) = B(\phi) \quad \forall \phi \in W_h. \end{aligned}$$

After finite element discretization, we end up with a large sparse linear system of equations that we solved with a preconditioned conjugate gradient method. As a preconditioner, we used an incomplete Cholesky decomposition, cf. e.g., [13], which was provided by Kaskade7.

The evaluation of the line integrals (16) is performed by numerical quadrature along the trajectory of u. As seen in Figure 2, the action potential is only nonzero on a small part of the trajectory but shows large oscillations there. Therefore, a standard composite quadrature on uniform intervals would be inefficient. To overcome this problem, we used an adaptive multigrid quadrature, cf. e.g., [6]. The necessary evaluation of the finite element function ω_h at a quadrature point x requires a search for the tetrahedron $K \in \mathcal{T}$ which contains x. To do this efficiently, we exploit that the quadrature points are ordered along the trajectory, and therefore we can use a neighborhood search. If this fails, we fall back to a hierarchic search over the whole grid.

In Figure 4a, we visualized the time dependent simulated signal on all 24 electrodes. For this simulation, we used a motor unit that is placed 4 mm below the electrodes. Depending on their location we observe quite a different behaviors. It can, for example, clearly be observed that electrodes that are placed distantly from the source measure weaker signals.

It is well known that the identification of the depth of a source is difficult when identifying sources from boundary measurements. We thus perform a variation in depth of the motor unit. In Figure 4b, we show the simulated measurement of one electrode (marked in red in Figure 4a) and for motor units with different depths. As one can see, most of the measured potential decreases very fast if the depth is increased. But due to the concentrated stationary sources, the potential decrease is much slower at the end of the measurement. That is a well known effect when modeling monopolar signals, see [10, 14].

Our approach reduces the required numerical effort for a simulation significantly. For our simulation, we divided a time interval into 200 time steps. That means, with the classical approach, we would have to solve a PDE 200 times. Using our adjoint approach, we only have to solve a PDE as much as there are electrodes. In our example, this is 24 times. Therefore we reduced the numerical effort for solving the PDE by a factor of 8. If one would solve the optimal control problem, which we introduce in the next section, the factor becomes much bigger, since there one would have to solve the PDE in each optimization step 200 times.

3 Identification of a Motor Unit from Measurements

In this section we will specify the identification problem which we want to solve. It is an inverse problem in the following sense: up to now, the motor unit was modeled as the trace of a given curve u and we derived a model for the simulation of the measurements $y_i(u,t)$ at n_E electrodes. From now on, we assume that measurements $y_{m,i}(t)$ are available and we are looking for a curve u, such that the corresponding simulated values $y_i(u,t)$ and the measurements $y_{m,i}(t)$ fit well. Collecting all these measurements and simulations in the vectors $y(t), y_m(t) \in \mathbb{R}^{n_E}$ and using the standard Euclidean norm $\|\cdot\|_{n_E,2}$ on $\mathbb{R}^{n_E}$, this leads to the following least-squares type tracking term

$$J_1(u) = \frac{1}{2} \int_0^T \|y(u,t) - y_m(t)\|_{n_E,2}^2 \, \mathrm{d}t.$$

By inspection of the given measurement y_m and the subdomains of Ω, one can obtain a rough estimate of where the motor unit u is located. Thus, we can choose a reference trajectory u_{ref} (e.g. a piecewise linear curve that connects the estimated location of the neuromuscular junction and the end-plates) a prior and add the following regularization term to the problem (where $\|\cdot\|_2$ is the standard Euclidean norm on $\mathbb{R}^3$):

$$J_2(u) := \frac{\alpha_1}{2} \int_{-1}^1 \|u(\tau) - u_{\mathrm{ref}}(\tau)\|_2^2 \, \mathrm{d}\tau.$$

Additionally, we assume that motor units are smooth in healthy tissue and therefore we add a second regularization term, which is given through

$$J_3(u) := \frac{\alpha_2}{2} \int_{-1}^1 \|\ddot{u}(\tau)\|_2^2 \, \mathrm{d}\tau.$$

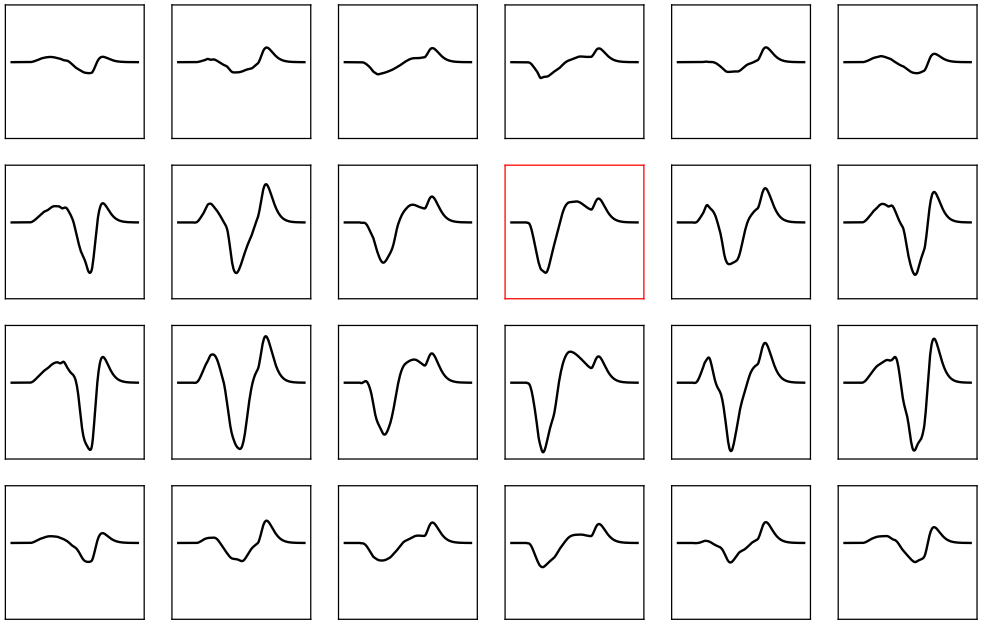

(a) Simulated measurement on a 6x4 electrode grid. The geometric configuration corresponds to the one, shown in Figure 3. The curves show the temporal behavior of the measured potential.

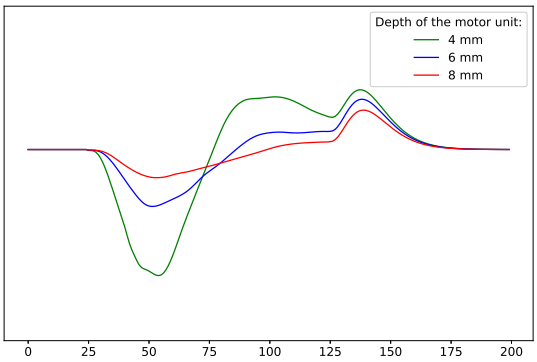

(b) Impact of the motor unit depth on the simulated measurement

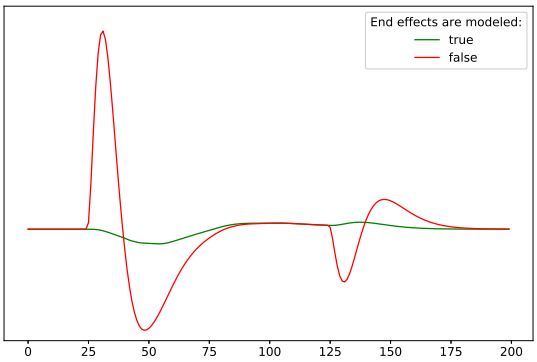

(c) Comparison of an surface EMG simulation with (green) and without (red) correction of end effects

Figure 4: Simulated measurement for a single fibered motor unit

This term also yields the necessary compactness the show existence of optimal solutions.

Finally, we will add a constraint which ensures that the signal passes the motor unit with constant speed $\nu > 0$, as assumed in section 2.4. Therefore, we define the constraint function

$$\begin{aligned} G : H^2(-1,1,\mathbb{R}^3) &\mapsto H^1(-1,1,\mathbb{R}) \\ [G(u)](\tau) &:= \|\dot{u}(\tau)\|_2^2 - \nu^2, \end{aligned} \tag{17}$$

and demand that $[G(u)](\tau) = 0$ for almost every $\tau \in [-1,1]$. We also demand that the solution is located in the muscle tissue $\overline{\Omega}_M$. Combining those two constraints, we get the following

admissible set

$$U_{ad} := \{v \in H^2(-1,1,\mathbb{R}^3) \,|\, v(\tau) \in \overline{\Omega}_M,\ G(v)(\tau) = 0,\ \text{for a. e. } \tau \in [-1,1]\}. \tag{18}$$

We note that this definition of the admissible set makes sense, due to the fact that $H^2(-1,1,\mathbb{R}^3)$ is embedded in $C^1(-1,1,\mathbb{R}^3)$. Collecting everything we get the optimization problem

$$\min_{u \in U_{ad}} J(u) := J_1(u) + J_2(u) + J_3(u). \tag{19}$$

Alternatively, we can write this problem as an unconstrained problem by adding an indicator function, such that we get

$$\min_{u \in H^2(-1,1,\mathbb{R}^3)} F(u) := J(u) + \iota_{U_{ad}}(u). \tag{20}$$

Now that we have derived a identification problem, we want to know if the problem has a solution.

Remark 2. *Some straightforward extensions of this identification problem are conceivable: for example we may add the speed ν to the set of variables, to be identified, and similarly the scaling parameter a. For simplicity of presentation we assume these parameters to be given.*

3.1 Existence of a solution

To prove that the problem has at least one solution, we first need some auxiliary results. First we show that the admissible set is weakly closed and that the equality constraint satisfies enough regularity. The second result shows that the functional J is differentiable and weakly lower continuous. We use then this two results two show that the objective functional satisfies the properties that we need to proof the existence result. The first auxiliary lemma is:

Lemma 3.1. *The admissible set U_{ad} is weakly closed and the equality constraint G is Fréchet differentiable.*

Proof. To show that U_{ad} is weakly closed, it is sufficient to show that the set

$$U_1 = \{v \in H^2(-1,1,\mathbb{R}^3) |\, v(\tau) \in \overline{\Omega}_M \text{ for a.e } \tau \in [-1,1]\}$$

and

$$U_2 = \{v \in H^2(-1,1,\mathbb{R}^3) |\, G(v)(\tau) = 0 \text{ for a. e. } \tau \in [-1,1]\}$$

are weakly closed. The admissible set U_{ad} is then as intersection of finitely many sets also weakly closed.

Let $u : [-1,1] \mapsto \overline{\Omega}_M$ be a regular curve. From [5, Theorem 8.8] it follows that a compact embedding $E_1 : H^2(-1,1,\mathbb{R}^3) \mapsto C(-1,1,\mathbb{R}^3)$ exist, and thus one can find a $v \in H^2(-1,1,\mathbb{R}^3)$ such that $E_1 v = u$. Thus U_1 is well defined and not empty.
Let now $\{u_k\} \subset U_1$ be a weak convergent sequence with limit u. Since the embedding E_1 is compact there exist a subsequence u_{k_l} such that $E_1 u_{k_l} \to E_1 u$ in $C(-1,1,\mathbb{R})$. Furthermore, there exist a another subsequence $E_1 u_{k_{l_i}}$ that converges pointwise to $E_1 u$ for all $\tau \in [-1,1]$. Since $\overline{\Omega}$ is closed and $E_1 u_{k_{l_i}}(\tau) \in \overline{\Omega}$ it follows that $E_1 u(\tau) \in \overline{\Omega}$ and thus also $u(\tau)$. This shows that U_1 is weakly closed.

As above there exits a compact embedding $E_2 : H^1(-1,1,\mathbb{R}^3) \mapsto W^{1,4}(-1,1,\mathbb{R}^3)$ with $E_2 \dot{u} = \dot{u}$. From Hölder's inequality it follows that $\langle \dot{u}, \dot{u} \rangle_2 \in H^1(-1,1,\mathbb{R})$ and thus

$$\begin{aligned} G :& H^2(-1,1,\mathbb{R}^3) \mapsto L^2(-1,1,\mathbb{R}) \\ [G(u)](\tau) &= \langle \dot{u}(\tau), \dot{u}(\tau) \rangle_2 - \nu^2 \end{aligned}$$

is well defined. It is well known that, as a continuous bilinear form, G is Fréchet differentiable with derivative

$$[G'(u)(v)](\tau) = \langle \dot{u}(\tau), \dot{v}(\tau) \rangle_2.$$

Let now $\{u_k\} \subset U_2$ be a weak convergent sequence with limit u. As above there exist a subsequence u_{k_l} such that $Eu_{k_l} \to Eu$ in $L^4(-1,1,\mathbb{R}^3)$. Since G is differentiable it is also continuous. That means that

$$0 = G(Eu_{k_l}) \to G(Eu),$$

□

which shows that U_2 is weakly closed.

Next we show the following Lemma:

Lemma 3.2. *The functional $J : H^2(-1,1,\mathbb{R}^3) \supset U_{ad} \mapsto \mathbb{R}$ is continuous, and weakly lower semi-continuous. If $u(\tau) \in \Omega_M$ for all $\tau \in [-1,1]$, then J is Fréchet differentiable at u.*

Proof. First we note that, as a sum, J is continuous, Fréchet differentiable and weakly lower semi-continuous, if J_1 and J_2 are continuous, Fréchet differentiable and weakly lower semi-continuous. To show the three properties for J_1, we define for fixed t and k the mapping

$$\begin{aligned} \psi_k &: \Omega_M \times [-1,1] \mapsto \mathbb{R} \\ \psi_k(x,\tau) &:= \omega_k(x) \nu \hat{\rho}_l(\tau, t). \end{aligned}$$

with derivative

$$\begin{aligned} \psi_{k,x} &: \Omega_M \times [-1,1] \mapsto \mathcal{L}(\mathbb{R}^3, \mathbb{R}) \\ \psi_{k,x}(x,\tau)v &:= \langle \nabla \omega_k(x), v \rangle_2 \nu \hat{\rho}_l(\tau, t). \end{aligned}$$

From Lemma 2.2 we now that $\omega_k : \Omega_M \mapsto \mathbb{R}$ is in $C^\infty(\Omega_M)$ and therefore also $\nabla \omega_k \in C^\infty(\Omega_M)$. Thus it follows that $\psi_k(\cdot,\tau)$ and $\psi_{k,x}(\cdot,\tau)$ are continuous for all $\tau \in [-1,1]$. Thus ψ_k is Fréchet differentiable, see [34, Page 192].
From [2, Theorem 6.3 and 6.7] we know that the corresponding superposition operator Ψ_k maps $C(-1,1,\mathbb{R}^3)$ into itself if ψ_k is continuous and is Fréchet differentiable if ψ_k is Fréchet differentiable. Furthermore, we know from [5, Theorem 8.8] that there exist a continuous compact embedding $E : H^2(-1,1,\mathbb{R}^3) \mapsto C(-1,1,\mathbb{R}^3)$ with $Eu = u$. Thus, it follows that the superposition operator

$$\begin{aligned} \Psi_k &: U_{ad} \mapsto C(-1,1,\mathbb{R}^3) \\ (\Psi_k(u))(\tau) &:= \psi_k(Eu(\tau), \tau) \end{aligned}$$

is well defined and Fréchet differentiable with derivative

$$\begin{aligned} \Psi_k' &: U_{ad} \mapsto \mathcal{L}\left(H^2(-1,1,\mathbb{R}^3); C(-1,1,\mathbb{R})\right) \\ (\Psi_k'(u)v)(\tau) &= \psi_{k,x}(Eu(\tau), \tau) Ev(\tau). \end{aligned}$$

With the same argumentation it follows that the correction terms $\omega_k(u(\cdot))I_m(\cdot)$ are well defined and Fréchet differentiable. Thus it follows immediately that

$$y_k(u,t) = \int_{-1}^{1} \Psi_k(u)(\tau)\, \mathrm{d}\tau + 2\omega_k(u(0)) I_m(\nu \cdot (t_0 - t)) - (\omega_k(u(-1)) + \omega_k(u(1)) I_m(\nu \cdot (t_1 - t))$$

is well defined and Fréchet differentiable with derivative

$$D_u y_k(u,t)(v) = \int_{-1}^{1} \langle \nabla \omega_k(u(\tau)), v(\tau) \rangle_2 \nu \hat{\rho}_l(\tau, t)\, \mathrm{d}\tau + 2\langle \nabla \omega(u(0)), v(u(0)) \rangle_2 I_m(\nu \cdot (t_0 - t)) \\ - \left(\langle \nabla \omega_k(u(-1)), v(u(-1)) \rangle_2 + \langle \nabla \omega_k(u(1)), v(u(1)) \rangle_2 \right) I_m(\nu \cdot (t_1 - t)).$$

Using the chain rule it follows that $J_1(u) = \frac{1}{2} \int_0^T \|y(u,t) - y_m(t)\|^2_{n_E,2}\, \mathrm{d}t$ is Fréchet differentiable with derivative $J_1'(u)(v) = \int_0^T \langle y(u,t) - y_m(t), D_u y(u,t)(v) \rangle_{n_E,2}\, \mathrm{d}t$.
Finally, since $J_1 : C(-1,1,\mathbb{R}^3) \mapsto C(-1,1,\mathbb{R}^3)$ is differentiable, it is also continuous and especially lower semi-continuous in $C(-1,1,\mathbb{R}^3)$. Furthermore we know that the embedding $E : H^2(-1,1,\mathbb{R}^3) \mapsto C(-1,1,\mathbb{R}^3)$ is compact, and thus it follows that J_1 is weakly lower semi-continuous in $H^2(-1,1,\mathbb{R}^3)$.

J_2 and J_3 are obviously convex quadratic bilinear forms. Thus it is well known that they are Fréchet differentiable from L_2 into itself and weakly lower semi-continuous, cf. e.g. [9]. The derivatives of J_2 and J_3 are then given through

$$J_2'(u)v = \int_{-1}^{1} \alpha_1 \langle u(\tau) - u_{\mathrm{ref}}(\tau), v(\tau) \rangle_2\, \mathrm{d}\tau \text{ and}$$

$$J_2'(u)v = \int_{-1}^{1} \alpha_2 \langle \ddot{u}(\tau), \ddot{v}(\tau) \rangle_2\, \mathrm{d}\tau.$$

Using the sum rule it follows that J is continuous and Fréchet differentiable and since the lim inf is super-additive, J is weakly lower semi-continuous. □

Collecting the derivatives from the previous proof, we get for the derivative J

$$J'(u)v = \int_0^T \langle y(u,t) - y_m(t), D_u y(u,t)(v) \rangle_{n_E,2}\, \mathrm{d}t \\ + \int_{-1}^{1} \alpha_1 \langle u(\tau) - u_{\mathrm{ref}}(\tau), v(\tau) \rangle_2 + \alpha_2 \langle \ddot{u}(\tau), \ddot{v}(\tau) \rangle_2\, \mathrm{d}\tau.$$

Remark 3. *Recall that the derivatives $\nabla\omega(x)$, required in the definition of $D_u y(u,t)$ are well defined by Lemma 2.2, since u is assumed to be contained in the muscular tissue Ω_M. However, if ω is approximated by a finite element function, $\nabla\omega$ is only piecewise continuous.*

The last auxiliary result is:

Lemma 3.3. *The objective functional F is weakly lower semi-continuous and radially unbounded.*

Proof. From Lemma 3.2 we already now that J is weakly lower semi-continuous. Thus, it remains two show that the indicator function is lower semi-continuous.

A function $f : X \mapsto \mathbb{R}$ is weakly lower semi-continuous if the level sets $N_\alpha f = \{x \in X | f(x) \leq \alpha\}$ are weakly closed for all $\alpha \in \mathbb{R}$, see [7, Theorem 7.4.11]. For the indicator function the level sets are given through

$$N_\alpha \iota_{U_{ad}}(u) = \begin{cases} U_{ad} & \text{if } \alpha > 0 \\ \emptyset & \text{else.} \end{cases}$$

From Lemma 3.1 we know that U_{ad} is weakly closed and since the empty set is always weakly closed it follows that the indicator function is weakly lower semi-continuous.

Obviously we have that $F(u) > 0$ and for $\|u\|_{2,2} \to \infty$ either J_2,J_3 or $\iota_{U_{ad}}$ goes to infinity. Thus it follows immediately that F is radially unbounded. □

Using this three auxiliary results, we can proof the following existence result:

Theorem 3.4. *The optimization problem* (20) *has at least one solution.*

Proof. Let $\{u_n\}$ be a minimizing sequence in the level sets N_α. From Lemma 3.3 we know that F is radially unbounded and therefore the level sets N_α are bounded for all $\alpha \in \mathbb{R}$, i.e. u_n is bounded. Since $H^2(-1, 1, \mathbb{R}^3)$ is reflexive, there exist a weakly convergent subsequence u_{n_k} with limit u_*. From Lemma 3.3 we also know that F is weakly lower semi-continuous and thus

$$\inf F \leq F(u_*) \leq \liminf F(u_{n_k}) = \inf F,$$

which shows that the limit point u_* is a minimizer of F. □

3.2 First-Order Optimality Conditions

Now that we know that at least one solution to the problem (19) exist, we derive first-order conditions for the problem. This is complicated by the geometric constraint $u \subset \overline{\Omega}_M$, which we imposed to assert existence of solution. However, from a practical point of view, we can expect that the optimal solution u_* is contained in Ω_M without the need to enforce this as a constraint, because the measured values orginate form a true signal, emitted from Ω_M. In addition, the objective functional is penalized by J_2 if u is too far away from a reference curve u_{ref}, which lies in Ω_M. Therefore, for simplictiy, we will drop these constraints from now on, and assume the optimal solutions u_* lies in the muscle domain Ω_M. That means we can rewrite the optimal control problem 19 as a pure equality constrained problem:

$$\begin{aligned} &\min_{u \in H^2(-1,1,\mathbb{R}^3)} J(u) \\ &\text{s.t.} \quad G(u)(\tau) = 0 \quad \text{for a. e. } \tau \in [-1, 1]. \end{aligned} \tag{21}$$

As usual we eliminate the equality constraint with the help of a Lagrange multiplier, which lead to the following result:

Theorem 3.5. *Let u_* be a local minimizer of* (21) *that lies in Ω_M. Then there exist a Lagrange multiplier $\lambda \in H^1(-1, 1, \mathbb{R})$, such that*

$$\begin{aligned} 0 &= J'(u_*) + G'(u_*)^* \lambda \\ 0 &= G(u_*)(\tau) \quad \textit{for a. e. } \tau \in [-1, 1] \\ \lambda &\in H^1(-1, 1, \mathbb{R})^* \end{aligned} \tag{22}$$

Proof. First, we recall that $\lambda \in H^1(-1,1,\mathbb{R})^*$ is called Lagrange multiplier, if

$$\begin{aligned}
&\lambda \in K^+ \\
&\lambda\left(G(u_*)\right) = 0 \\
&J'(u_*) - G'(u_*)^*\lambda \in C(u_*)^+
\end{aligned}$$

is fulfilled, cf. [35, Eq. 1.1]. Here K is a convex closed cone such that $G(u) \in K$ and K^+ is the dual cone of K. Since we have pure equality constraints, $K = \{0\} \subset H^1(-1,1,\mathbb{R})$ and from the definition of the dual cone it follows that $K^+ = H^1(-1,1,\mathbb{R})^*$, see [30, 35]. From the $\left[G(u_*)\right](\tau) = 0$ it follows that the second condition is always fulfilled and thus we can replace it by $\left[G(u_*)\right](\tau) = 0$. Furthermore, $C(u_*)$ is the conical hull of $H^2(-1,1,\mathbb{R}^3)$, which is $H^2(-1,1,\mathbb{R}^3)$ and therefore the dual cone $C(u_*)^+ = \{0\}$. Thus, the third condition simplifies to

$$J'(u_*) - G'(u_*)^*\lambda = 0.$$

Since we already know from Lemma 3.2 that J and G are Fréchet differentiable, it follows from [30, Theorem 6.3] that a Lagrange multiplier λ exists, if G satisfies the regularity condition of Zowe and Kurcyusz, which is given through

$$G'(u_*)C(u_*) + K(-G(u_*)) = H^1(-1,1,\mathbb{R}).$$

Here $K(\cdot)$ is the convex hull of K. From $K = \{0\}$ and $G(u_*) = 0$ it follows that $K(G(u_*)) = \{0\}$ and since $C(u_*) = H^2(-1,1,\mathbb{R}^3)$, this condition is equivalent to $G'(u_*)$ surjective. To show this, we choose for arbitrary $w \in H^1(-1,1,\mathbb{R})$

$$v(\tau) = \int_{-1}^{\tau} \frac{\dot{u}_*(\xi)w(\xi)}{\nu^2}\,\mathrm{d}\xi,$$

which is in $H^2(-1,1,\mathbb{R}^3)$ and has the derivative

$$\dot{v}(\tau) = \frac{\dot{u}_*(\tau)w(\tau)}{\nu^2}.$$

It yields then

$$\left[G'(u_*)(v)\right](\tau) = \langle \dot{u}_*(\tau), \frac{\dot{u}_*(\tau)w(\tau)}{\nu^2}\rangle_2 = w(\tau)\frac{\langle \dot{u}_*(\tau), \dot{u}_*(\tau)\rangle_2}{\nu^2} = w(\tau)$$

and since $w \in H^1(-1,1,\mathbb{R})$ was arbitrary it follows that $G'(u_*)$ is surjective. □

From the definition of an adjoint operator it follows that $G'(u_*)^*\lambda = \lambda(G'(u_*))$ where λ is a linear functional and therefore we can write the KKT condition (22) as

$$\begin{aligned}
0 &= \int_0^T \langle y(u,t) - y_m(t), D_u y(u,t)\delta u(t)\rangle_{n_E,2}\,\mathrm{d}t + \lambda(\langle \dot{u}, \delta\dot{u}\rangle_2) \\
&\quad + \int_{-1}^{1} \alpha_1\langle u(\tau) - u_{\mathrm{ref}}(\tau), \delta u(\tau)\rangle_2 + \alpha_2\langle \ddot{u}(\tau), \delta\ddot{u}(\tau)\rangle_2\,\mathrm{d}\tau \quad \forall \delta u \in H^2(-1,1,\mathbb{R}^3) \\
0 &= \|\dot{u}(\tau)\|_2^2 - \nu^2 \quad \text{for a.e. } \tau \in [-1,1] \\
\lambda &\in H^1(-1,1,\mathbb{R})^*
\end{aligned} \tag{23}$$

with

$$D_u y(u,t)(v) = \int_{-1}^{1} \langle \nabla\omega(u(\tau)), v(\tau)\rangle_2 \nu \hat{\rho}_l(\tau,t)\,\mathrm{d}\tau + 2\langle \nabla\omega(u(0)), v(u(0))\rangle_2 I_m(\nu(t_0-t))$$
$$- \left(\langle \nabla\omega(u(-1)), v(u(-1))\rangle_2 - \langle \nabla\omega(u(1)), v(u(1))\rangle_2\right) I_m(\nu(1+t_0-t))$$

These first order optimality conditions will be the basis of a computational approach that will be elaborated in a forthcoming paper.

References

[1] S. Andreassen and A. Rosenfalck, *Relationship of intracellular and extracellular action potentials of skeletal muscle fibers*, Critical Reviews in Bioengineering **6** (1981), no. 4, 267–306.

[2] Jürgen Appell and Petr Petrovič Zabrejko, *Nonlinear superposition operators*, Cambridge tracts in mathematics, vol. 95, Cambridge Univ. Press, Cambridge, 1990.

[3] Peter Bastian, Markus Blatt, Andreas Dedner, Nils-Arne Dreier, Christian Engwer, René Fritze, Carsten Gräser, Christoph Grüninger, Dominic Kempf, Robert Klöfkorn, Mario Ohlberger, and Oliver Sander, *The Dune framework: Basic concepts and recent developments*, Computers & Mathematics with Applications **81** (2021), 75–112.

[4] Blender Online Community, *Blender - a 3D modelling and rendering package*, 2021.

[5] Haim Brezis, *Functional Analysis, Sobolev Spaces and Partial Differential Equations*, Universitext, Springer Science+Business Media LLC, New York, NY, 2010.

[6] Peter Deuflhard and Andreas Hohmann, *Numerical Analysis in Modern Scientific Computing: An Introduction*, second edition ed., Texts in Applied Mathematics, vol. 43, Springer, New York, NY, 2003.

[7] Jacques Dixmier, *General Topology*, Undergraduate Texts in Mathematics, Springer, New York, NY, 1984.

[8] Manfred Dobrowolski, *Angewandte Funktionalanalysis: Funktionalanalysis, Sobolev-Räume und elliptische Differentialgleichungen*, 2., korrigierte und überarb. aufl. ed., Springer, Berlin, 2010.

[9] Ivar Ekeland and Roger Temam, *Convex analysis and variational problems*, unabridged, corr. republ ed., Classics in applied mathematics, vol. 28, SIAM, Philadelphia, 1999.

[10] Dario Farina, Corrado Cescon, and Roberto Merletti, *Influence of anatomical, physical, and detection-system parameters on surface EMG*, Biological Cybernetics **86** (2002), no. 6, 445–456.

[11] Christophe Geuzaine and Jean-François Remacle, *Gmsh: A 3-D finite element mesh generator with built-in pre- and post-processing facilities*, International Journal for Numerical Methods in Engineering **79** (2009), no. 11, 1309–1331.

[12] David Gilbarg and Neil S. Trudinger, *Elliptic partial differential equations of second order*, reprint of the 1998 ed. ed., Classics in mathematics, Springer, Berlin, 2001.

[13] Gene H. Golub and Charles F. van Loan, *Matrix computations*, 4. ed. ed., Johns Hopkins studies in mathematical sciences, Johns Hopkins Univ. Press, Baltimore, Md., 2013.

[14] T.H.J.M. Gootzen, D. F. Stegeman, and A. van Oosterom, *Finite limb dimensions and finite muscle length in a model for the generation of electromyographic signals*, Electroencephalography and Clinical Neurophysiology/Evoked Potentials Section **81** (1991), no. 2, 152–162.

[15] Sebastian Götschel, Martin Weiser, and Anton Schiela, *Solving Optimal Control Problems with the 5K6askade7 Finite Element Toolbox*, Advances in Dune, Springer, Berlin, 2012, pp. 101–112.

[16] Roberta Grech, Tracey Cassar, Joseph Muscat, Kenneth P. Camilleri, Simon G. Fabri, Michalis Zervakis, Petros Xanthopoulos, Vangelis Sakkalis, and Bart Vanrumste, *Review on solving the inverse problem in EEG source analysis*, Journal of neuroengineering and rehabilitation **5** (2008), 25.

[17] R. Haller-Dintelmann, C. Meyer, J. Rehberg, and A. Schiela, *Hölder Continuity and Optimal Control for Nonsmooth Elliptic Problems*, Appl Math Optim **60** (2009), no. 3, 397–428.

[18] Michael Hinze, Rene Pinnau, Michael Ulbrich, and Stefan Ulbrich, *Optimization with PDE constraints*, Mathematical modelling, vol. 23, Springer, Dordrecht, 2009.

[19] Bert U. Kleine, Johannes P. van Dijk, Bernd G. Lapatki, Machiel J. Zwarts, and Dick F. Stegeman, *Using two-dimensional spatial information in decomposition of surface EMG signals*, Journal of Electromyography and Kinesiology **17** (2007), no. 5, 535–548.

[20] Yang Liu, Yong Ning, Sheng Li, Ping Zhou, William Z. Rymer, and Yingchun Zhang, *Three-Dimensional Innervation Zone Imaging from Multi-Channel Surface EMG Recordings*, International Journal of Neural Systems **25** (2015), no. 6, 1550024.

[21] M. M. Lowery, *EMG Modeling and Simulation: 8*, Surface Electromyography : Physiology, Engineering, and Applications, John Wiley & Sons, Ltd, 2016, pp. 210–246.

[22] Jaakko Malmivuo and Robert Plonsey, *Bioelectromagnetism: Principles and applications of bioelectric and biomagnetic fields*, Oxford Univ. Press, New York, NY, 1995.

[23] Luca Mesin, *Real time identification of active regions in muscles from high density surface electromyogram*, Computers in Biology and Medicine **56** (2015), 37–50.

[24] Christian Meyer, Lucia Panizzi, and Anton Schiela, *Uniqueness Criteria for the Adjoint Equation in State-Constrained Elliptic Optimal Control*, Numerical Functional Analysis and Optimization **32** (2011), no. 9, 983–1007.

[25] Diego Pereira Botelho, Kathleen Curran, and Madeleine M. Lowery, *Anatomically accurate model of EMG during index finger flexion and abduction derived from diffusion tensor imaging*, PLOS Computational Biology **15** (2019), no. 8, e1007267.

[26] R. Plonsey and D. B. Heppner, *Considerations of quasi-stationarity in electrophysiological systems*, The Bulletin of Mathematical Biophysics **29** (1967), no. 4, 657–664.

[27] P. Rosenfalck, *Intra- and extracellular potential fields of active nerve and muscle fibres. A physico-mathematical analysis of different models*, Acta Physiologica Scandinavica. Supplementum **321** (1969), 1–168.

[28] Guido Stampacchia, *Le problème de Dirichlet pour les équations elliptiques du second ordre à coefficients discontinus*, Annales de l'institut Fourier **15** (1965), no. 1, 189–257.

[29] Dick F. Stegeman, Joleen H. Blok, Hermie J. Hermens, and Karin Roeleveld, *Surface EMG models: properties and applications*, Journal of Electromyography and Kinesiology **10** (2000), no. 5, 313–326.

[30] Fredi Tröltzsch, *Optimal control of partial differential equations: Theory, methods, and applications*, Graduate studies in mathematics Applied mathematics, vol. 112, American Math. Soc, Providence, RI, 2010.

[31] Kees van den Doel, Uri M. Ascher, and Dinesh K. Pai, *Computed myography: three-dimensional reconstruction of motor functions from surface EMG data*, Inverse Problems **24** (2008), no. 6, 065010.

[32] ———, *Source localization in electromyography using the inverse potential problem*, Inverse Problems **27** (2011), no. 2, 025008.

[33] J. P. van Dijk, M. M. Lowery, B. G. Lapatki, and D. F. Stegeman, *Evidence of potential averaging over the finite surface of a bioelectric surface electrode*, Annals of Biomedical Engineering **37** (2009), no. 6, 1141–1151.

[34] Eberhard Zeidler, *Nonlinear Functional Analysis and its Applications: III: Variational Methods and Optimization*, Springer New York, New York, NY and s.l., 1985.

[35] J. Zowe and S. Kurcyusz, *Regularity and stability for the mathematical programming problem in Banach spaces*, Appl Math Optim **5** (1979), no. 1, 49–62.